Check for updates

Three-dimensional electron diffraction: a powerful structural characterization technique for crystal engineering

Laura Samperisi, Xiaodong Zou [iD] and Zhehao Huang [iD] *

Understanding crystal structures and behaviors is crucial for constructing and engineering crystalline materials with various properties and functions. Recent advancement in three-dimensional electron diffraction (3D ED) and its application on structural characterizations have expanded single-crystal analysis into nano-sized materials. Herein, we provide an overview on 3D ED, including its development, data collection protocols, and their applications for investigating crystal structures. We focus on metal–organic frameworks (MOFs) and small-molecule-based organic crystals, and highlight the insights provided by 3D ED such as structure–property relationships, polymorphism, hydrogen bonding, and crystal chirality, which are crucial subjects in crystal engineering. With more and more laboratories setting up 3D ED techniques, we envision that it will not only continue providing critical structural information, but also establish a wide impact on chemistry, materials science and life science.

1. Introduction

Developing fast and reliable structure determination techniques is of paramount importance for the research of crystal engineering because structural information at an atomic level offers the fundamental understanding on crystal behaviors and structure–property relationships. Single-crystal X-ray diffraction (SCXRD) has been developed for more than one century.[1] It has been considered as a mature technique and the primary choice among those to study crystalline compounds,[2–4] such as metal–organic frameworks (MOFs) and organic crystals, which offer unique properties for applications in physical and life sciences.[5,6] Compared to neutron diffraction, diffractometers for X-ray crystallography are widely available and of easy access. High quality X-ray diffraction data can provide accurate coordinates and anisotropic displacement parameters (ADPs) in crystals, including examples of determining H atoms,[7] and the absolute configurations of chiral molecules.[8] However, as a critical requirement for SCXRD, crystals need to be larger than $5 \times 5 \times 5$ μm^3 in size. Powder X-ray diffraction (PXRD) has been used for studying crystals of smaller sizes, but peak overlap generated by large unit cells and/or multiple phases is often found challenging for structural analysis. Furthermore, controlling synthesis conditions to grow crystals of suitable size for SCXRD and to obtain sufficient phase purity for PXRD

are often raise additional challenges. Three-dimensional electron diffraction (3D ED) takes the unique advantage of the strong interaction between electrons and matter to allow investigations of crystals invisible to X-ray (*i.e.*, with $<5 \times 5 \times 5$ μm^3 in size).[9–12] Additionally, single-crystal analysis using 3D ED can be applied to study phase mixtures.[13]

3D ED measurements are typically conducted in a transmission electron microscope (TEM), which allows to obtain both diffraction and imaging data. Therefore, it is possible to evaluate crystal morphologies and collect single-crystal data on desired crystals, or randomly collecting data covering all the crystalline compounds coexisting in a sample. Since the first development of automated diffraction tomography (ADT)[14] and rotation electron diffraction (RED),[15] different 3D ED protocols have been independently developed including precession electron diffraction (PEDT),[16] continuous rotation electron diffraction (cRED),[17,18] electron diffraction tomography (EDT),[19] fast electron diffraction tomography (fast-EDT),[20] fast automated diffraction tomography (fast-ADT),[21] low-dose electron diffraction tomography (LD-EDT)[22] and microcrystal electron diffraction (MicroED).[23] These protocols are similar in sharing the concept that a series of electron diffraction patterns are recorded from a crystal tilted around the goniometer axis. While reciprocal space was first sampled discretely by stepwise rotation of a crystal, the development of fast detectors enabled the continuous recording of 3D ED data, and thus a continuous sampling of reciprocal space. As an additional advantage of continuous recording, data collection time is reduced to a few minutes per crystal, which allows

Department of Materials and Environmental Chemistry, Stockholm University, Stockholm SE-106 91, Sweden. E-mail: zhehao.huang@mmk.su.se

structural analysis of beam sensitive materials and compounds.[17,23–28] To process 3D ED data, programs developed for X-ray diffraction and specifically for electron diffraction are used. *XDS*,[29] *iMosFlm*[30] *DIALS*[31] and *PETS*,[32] can be used to extract the intensities. When the data resolution is higher than 1.2 Å, similarly to SCXRD, 3D ED data can be used for *ab initio* structure determination *via* direct methods, simulated annealing, molecular replacement, and charge flipping using programs such as *SHELX*,[33] *SIR2019* (ref. 34) and *SUPERFLIP*.[35] The structural models are typically followed by least-squares refinement using *SHELXL*,[36–38] *JANA2006*,[39–41] *etc.* When the data resolution is low, 3D ED data can be used for obtaining structural information such as unit cell parameters and space groups. Combining with other characterization techniques and chemical knowledge, such structural information is crucial for solving structures of low-quality crystals.

Here, we highlight the potential of applying 3D ED to investigate structures when crystals are not suitable for characterizations by X-ray diffraction, with a focus on metal–organic frameworks (MOFs) and organic crystals. We describe how 3D ED methods can be used to elucidate structure–property relationships, polymorphism and phase mixtures, hydrogen bonding interactions, and crystal chirality, which are the areas that attract significant interests for crystal engineering. Moreover, we provide our perspectives on 3D ED for their future advances and potential applications.

2. Three-dimensional electron diffraction (3D ED) methods

2.1. Stepwise and continuous data collection protocols

The key concept of 3D ED is to collect a sequence of diffraction patterns from a crystal at different tilt angles by rotating the TEM goniometer. Two different setups are now being used in the 3D ED protocols: stepwise rotation and continuous rotation (Fig. 1).

In the stepwise methods, such as ADT, PEDT, and RED, missing wedges between ED frames lead to a discretely sampled reciprocal space. As a result, reflection intensities are difficult to model due to the missing information of the same reflection allocated in two sequential frames.[20] Using precession electron diffraction (PED) in ADT/PEDT[20,42–44] and fine electron beam tilting in RED[15,45] the missing

information between the fixed angular steps can be eliminated or reduced. LD-EDT[22] is a recently developed stepwise protocol, which allows minimizing beam damage and it samples the gaps between the steps by precession. The stepwise 3D ED techniques have successfully been applied to understand crystal structures where SCXRD cannot be applied.[45–52] However, electron beam can damage crystalline materials and compounds, *i.e.*, inorganic–organic hybrids, organic crystals, *etc.* For such beam sensitive compounds, beam damage significantly limits data resolution and quality, and leads to losing structural details that can be studied. Thus, other characterization techniques, such as PXRD, nuclear magnetic resonance (NMR) spectroscopy, *etc.*, are often used to validate the structural information obtained by stepwise 3D ED techniques. With the development of fast detectors,[53–57] the reciprocal space can be sampled continuously in the protocols including cRED, fast-ADT, fast-EDT and MicroED. With these methods, the electron diffractions are recorded over a desired exposure time while the TEM goniometer keep continuously rotating at a constant speed (Fig. 2). As a result, the intensities are integrated over the exposure time, and thus are more accurate. By using continuous rotation methods, data acquisition can be performed at a high goniometer rotation speed with an electron dose rate of less than 0.01 e^- s^{-1} $Å^{-2}$. With the crystals being illuminated for less than one minute, the beam damage can be drastically reduced. However, because of the design of TEM goniometers, where the eucentricity is changing during the rotation, the target crystal can move out of the illuminated area and break the collection process. This drifting issue can be overcome by applying a dynamic tracking routine in which the diffraction patterns are defocused at regular intervals to visualize the position of the crystals and track them back either manually or by dedicated software, *i.e.*, *Instamatic*.[58] The reposition step can be avoided by using a stable TEM goniometer, or using large selected
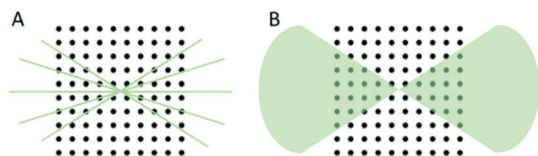

Fig. 1 Schematic illustration of (A) stepwise and (B) continuous rotation methods for 3D ED data collection. Stepwise methods sample the reciprocal space discretely with point intensities of the reflections are recorded. Continuous rotation methods sample the reciprocal space continuously and take an integral of the intensities over the exposure time.
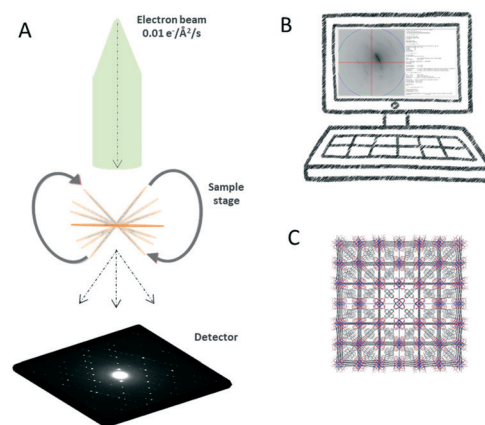

Fig. 2 Workflow of continuous rotation methods for 3D ED. (A) A fast camera records the diffraction patterns over a desired exposure time while the sample stage is continuously rotated under the electron beam. (B) The raw image data are processed to extract the intensities. (C) Structures of nanometer-sized crystals are solved *ab initio*.

area apertures. In the cases where crystals are severely aggregated, small selected area apertures are preferred to select an area without crystal overlap. Despite the high coverage of the reciprocal space of the continuous methods, the angular range of the TEM goniometer in a standard setup is limited to *ca.* 120°. Therefore, a missing cone is present and highly complete dataset from individual crystals could be difficult to obtain, especially in case of crystals with low symmetry. Merging electron diffraction data have been proved as an effective method for tackling this drawback.[59,60]

While dynamical effects occur in 3D ED data due to multiple scattering events, the rotation of the crystal through a range of arbitrary orientations can effectively reduce such effects. Moreover, the continuous coverage of the reciprocal space, and more accurately measured intensities can improve the accuracy for structure determination.[61,62] Despite the intensities are treated as kinematical approximation, and the resulting high R_1 values of electron data compared to X-rays, several studies have proven that the final structural models obtained by 3D ED and SCXRD are in good agreement even in the finest details.[59,61–65] It is worth mentioning that recently developed dynamical refinement[66,67] has been applied to 3D ED data and the R_1 values can be reduced.

2.2. Sample preparation

As a method for single-crystal analysis, 3D ED is used to determine structures of each individual crystal from phase mixtures. Crystals do not require to be individually prepared and mounted because multiple crystals can be deposited on a TEM grid for analysis. Sample preparation methods can be tailored to suit different variety of crystals. The most common method consists of crushing the powder sample at room temperature in a mortar and making a suspension in a volatile solvent (*i.e.*, EtOH, acetone, H_2O, cyclohexane, *etc.*). The resulting suspension can be deposited onto a TEM grid. After a complete evaporation of the solvent, the grid can be loaded to a TEM holder. This method is widely used for crystals that are stable in air and do not dissolve or lose crystallinity in the solvent. Without using solvents, alternatively, the crushed powder sample is picked up and loaded to glow discharged TEM grid. When low amount of sample is available, the grinding can be performed between two glass-coverslips.

Preventing vacuum damages is another crucial aspect for optimizing sample preparation procedures. For crystals stable in the air but sensitive to the high vacuum in TEM due to removal of guest species, the grid can be loaded on a cryo-transfer holder and the data collection can be performed at cryogenic temperatures. This strategy has been proven to be beneficial for the investigation of covalent-organic frameworks (COFs),[68] H-bonded organic frameworks (HOFs),[69] MOFs and zeolites.[70] For samples require to keep hydrated, aqueous suspension of the crystals is frozen at cryogenic temperatures to embed crystals in the ice. To make the ice thin enough for 3D ED measurement, methods such as plunge-freezing[71,72] and pre-assist method[73] are available, and they have been applied for study protein sub-microcrystals using 3D ED.

3. Applications of 3D ED

3.1. Structure–property relationships

As the properties of a compound is closely associate with its crystal structure, 3D ED has been applied to reveal the structural details and thus the physicochemical properties. The promising properties has been driving research in MOFs. This class of materials are known for their large surface areas, tunable pore architecture, structural flexibility and adjustable chemical functionality.[74] All these attributes make them appealing for a large variety of applications in heterogeneous catalysis,[75] gas adsorption–separation,[76] sensing,[77] energy storage and conversion,[78] and drug delivery,[79] *etc.* Thus, accurate structure determination is crucial for understanding their structures and functions. Despite MOFs are generally sensitive to electron beam damage, 3D ED methods have demonstrated to be a powerful technique complementary to SCXRD and PXRD for the structural analysis of MOF nanocrystals.[61–64,80–90] In this section, we describe examples in which 3D ED methods were valuable to analyze MOFs structures and reveal their properties.

Mesoporous MOFs represents a challenge for diffraction techniques due to their large structures often crystallizes in small and poorly diffracting crystals. PCN-333 (ref. 86) and PCN-777 (ref. 87) correspond to this description and their structures have been solved by combining the key information on unit cell and space group obtained from RED data and model building. Because these MOFs contain large cavities, they have advantages for encapsulation of enzymes. Another example of mesoporous MOF in which the application of the RED method was crucial for solving the structure and derive the properties is PCN-128W.[88] The unique topology of PCN-128W allows the 4′,4‴,4⁗,4⁗′-(ethene-1,1,2,2-tetrayl)tetrakis (([1,1′-biphenyl]-4-carboxylicacid)) linker (ETTC) to open and close when the compression is released and applied, respectively. This reversible structure change upon and external stimuli confers to the property of changing color and luminescence, thus making it as a piezofluorochromic MOF.

Thanks to the development of the continuous data acquisition, the beam damage to MOFs is minimized, and more structure have been determined *ab initio* by using 3D ED data. For example, CAU-23 (ref. 89) is a beam sensitive nano-sized MOF which has been solved *ab initio* by cRED (Fig. 3A). CAU-23 is a chiral MOF that crystallizes in a non-centrosymmetric space group. The structure consists in an inorganic building unit formed by repeating *cis* and *trans* corner-sharing AlO_6 polyhedra. The inorganic building units are connected through thiophenedicarboxylate (TDC) linkers.
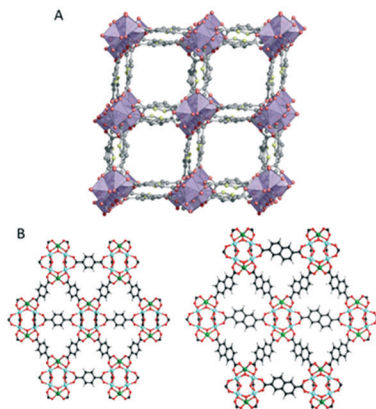
Fig. 3 (A) The structural model of CAU-23 viewing along the [010] direction. Purple polyhedrons: AlO_6; grey spheres: C; yellow spheres: N. Reproduced from ref. 89 with permission from *Nature Communication*, CC-BY license. (B) The structural models of PCN-415 and PCN-416. Cyan spheres: Zr; green spheres: Ti; red spheres: O; black spheres: C; grey spheres: H. Reproduced from ref. 90 with permission from the American chemical society, copyright 2019.

The opening angle between the two –COOH groups and the heteroatoms (oxygen or nitrogen) of the linker make the framework highly hydrophilic. This high-water sorption capacity even at low relative humidity makes CAU-23 an ideal candidate for ultra-low temperature water adsorption. PCN-415 and PCN-416 (ref. 90) are another example of MOF whose properties were revealed by cRED (Fig. 3B).

These two MOFs are isoreticular and both of them contain Ti(IV) and Zr(IV) cations in the frameworks; 1,4-benzenedicarboxylate (BDC) is used for the construction of PCN-415 while the framework of PCN-416 is linked by 2,6-naphthalenedicarboxylate (NDC). The structural insights provided by the high-resolution data could elucidate the photocatalytic mechanism in both MOFs by enabling the precise locations of Ti and Zr in the mixed metal cluster.

In addition to the structure–property relationships, 3D ED methods reported can be used to probe dynamic motions in MOFs.[63] Due to the high-quality cRED data, the structures of two Zr-MOFs, MIL-140C and UiO-67, coexisting in a mixture, were determined *ab initio*. By refining the ADPs, the
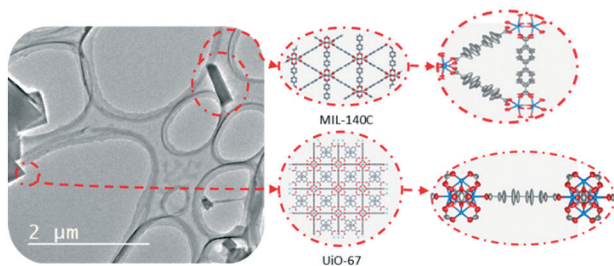
molecular motions of the linker molecules in both structures can be studied (Fig. 4). The linkers perform small amplitude librations along the molecular axis. Interestingly, in MIL-140C, different degrees of motions were observed depending on the local environment of the linker molecules. This study shows that 3D ED methods can offer valuable information for the analysis of dynamic changes.

3.2. Phase mixtures and polymorphs

3D ED has been demonstrated in several studies to be a fast and accurate method for single-crystal analysis of individual crystals in powder mixtures. One remarkable example is the structure determination of the ζ phase of the pigment red.[91] The structure solution of this pigment would only be possible by applying one of the 3D ED protocols, ADT, because of its low crystallinity and the presence of additional phases. The 3D ED protocol RED was also applied for phase identification and structure determination of four inorganic crystals in the Ni–Se–O–Cl system coexisting in mixture.[92] In addition, ADT could be used to independently characterize three bismuth sulfates, all of which were grown on the surface of bismuthinite.[93] With the development of the continuous 3D ED methods, the short data collection time facilitate high-throughput new material discovery in mixed phases. A recent study reports the structural analysis by cRED lead to
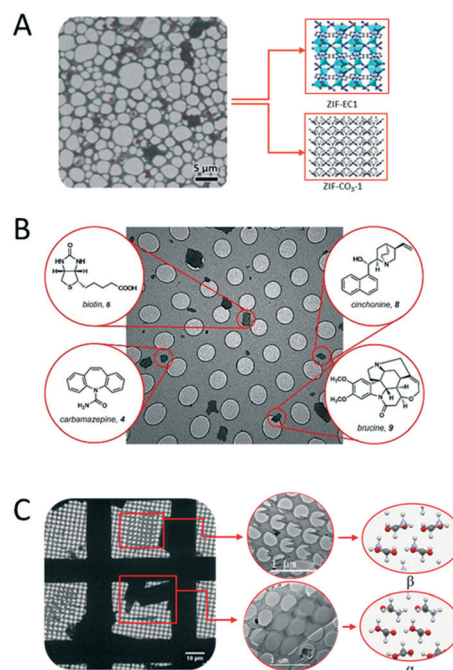

Fig. 5 Examples of distinct structures determined from phase mixtures by 3D ED. (A) Two MOFs of ZIF-EC1 and ZIF-CO$_3$-1. Adapted from ref. 94 with permission from the John Wiley & Sons, Inc., copyright 2021. (B) Four compounds of biotin, brucine, carbamazepine, and cinchonine. Reproduced from ref. 98 with permission from the American Chemical Society, copyright 2018. (C) Polymorphs of α- and β-glycine. Adapted from ref. 96 with permission from the International Union of Crystallography, copyright 2019.

Fig. 4 The structural models of MIL-140C and UiO-67 which are determined by 3D ED from a mixture. The refinement on ADPs using cRED data reveals small amplitude librations of the linker molecules. Modified from ref. 63 with permission from the American Chemical Society, copyright 2019.

discovering a new zeolitic-imidazolate frameworks (ZIF-EC1),[94] which has shown interesting electrocatalytic properties. The material was discovered as a minor phase in the crystalline powder with the already known ZIF-CO$_3$-1 (Fig. 5A). The serial rotation electron diffraction (SerialRED) method, developed by Wang *et al.*,[95] is another example to explore automated 3D ED method for structure determination of multiphasic nanocrystalline materials. The method was applied to determine structures of a mixture of zeolites, ZSM-5, ZSM-25, PST-20, and mordenite, and a MOF, PCN-416. This automated approach for crystal screening and cRED data collection can collect data from up to 500 crystals per hour for structure analysis.

3D ED has been applied for structural analysis of organic crystals.[13,96–104] Among them, the study of polymorphism is an area of significant interest in crystal engineering as it can provide precious insights into the factors responsible for molecular recognition and crystal packing.[105] Polymorphism has fundamental importance in the preparation and development of drugs. The majority of active pharmaceutical ingredient (API) exists in multiple polymorphic forms with different drug properties. Additionally, transitions between polymorphic forms are not unusual and can have dramatic effect. MicroED was applied for identification and structure determination of four natural compounds (biotin, carbamazepine, cinchonine and brucine) in a heterogeneous mixture (Fig. 5B), where all structures were solved to ~1 Å resolution.[98] Broadhurst *et al.*[96] applied the cRED method to study α, β and γ polymorphs of glycine crystals (Fig. 5C).

The polymorphs were crystallized *in situ* from a saturated aqueous solution on a TEM grid and each structure was solved and refined by using electron diffraction data. More recently, a combination of cryo-TEM and cRED allowed to identify the transient phases of the crystallization of carbamazepine.[97]

3.3. Hydrogen bonding interactions

One of the key studies in crystal engineering is to understand intermolecular interactions and use the obtained knowledge to control nucleation, crystal growth, and crystal structures. Knowing the primary structural motifs, *i.e.*, strong covalent interactions, oftentimes is not enough for crystal design because weaker interactions can dramatically affect the 3D packing such as shown by hydrogen bonding in peptide crystals. Given that hydrogen bond is one of the most encountered interactions, characterization methods capable of identifying hydrogen bonds are essential in crystal engineering. Using the 3D ED protocol PEDT with dynamical refinement, Palatinus *et al.*[106] reported direct localization of bonded and non-bonded hydrogen atoms in paracetamol (Fig. 6A) and cobalt aluminophosphate (CAP) (Fig. 6B). In this study, dynamical refinement improved single-to-noise ratio in difference potential maps from which all hydrogen atoms could be located in the paracetamol and CAP with their
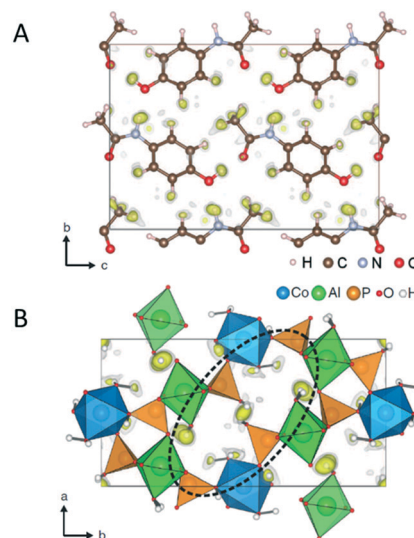

Fig. 6 The structural models and superimposed difference potential maps for identification of H atoms in (A) paracetamol, and (B) CAP. Reproduced from ref. 106 with permission from the American Association for the Advancement of Science, copyright 2017.

partial occupancy and disorder revealed. Clabbers *et al.*[107] localized hydrogen atoms of two pharmaceutical compounds, IRELOH (C$_{16}$O$_5$H$_{18}$) and EPICZA (C$_{18}$O$_6$N$_2$S$_2$H$_{16}$) by using kinematical approximation of cRED data. This study demonstrated that collecting data on nano-sized crystals with a highly sensitive hybrid pixel detector is an effective combination for minimizing dynamical scattering. With this approach, the positions of individual hydrogen atoms and the hydrogen–oxygen bond length could be determined and freely refined without any modelling of dynamical scattering.

Without directly locating hydrogen atoms, the detailed structural insights obtained by cRED data revealed hydrogen bonds in several structures. For example, hydrogen bonds between carboxylic acid groups on neighboring rods were individuated in the structure of a coordination compound bismuth subgallate[17] (Fig. 7A). Moreover, MOF CAU-45 (ref. 108) exhibits a honeycomb layered structure with large hexagonal-shaped channels, and from the refinement against cRED data it was possible to identify hydrogen bonds from the N–H donors and C=O acceptors, which enforce the layers to form a 3D structure (Fig. 7B). By using cRED, the structure of the HOF ABTPA-2 (ref. 69) was determined to be composed by 2D hydrogen bond networks layered in an A–B stacking arrangement, and the 1D structure of mCOF-Ag (ref. 109) was found to be stabilized by the H⋯F hydrogen bonding between amines and BF$_4^-$ anions. In a new series of hydroxamate-based MOFs, M-HAF-2 (M = Fe, Ga or In),[110] the first example of structure between a MOF and a HOF, hydrogen bonds were identified between metal-coordinated and uncoordinated hydroxamate groups. In the structural study of using cRED for MOF Co-CAU-36,[61] which was synthesized in a solvent mixture of 1,4-diazabicyclo[2.2.2]-octane (DABCO), HCl and water, hydrogen bonds were identified from the typical distances (NH⋯O) and (OH⋯O)
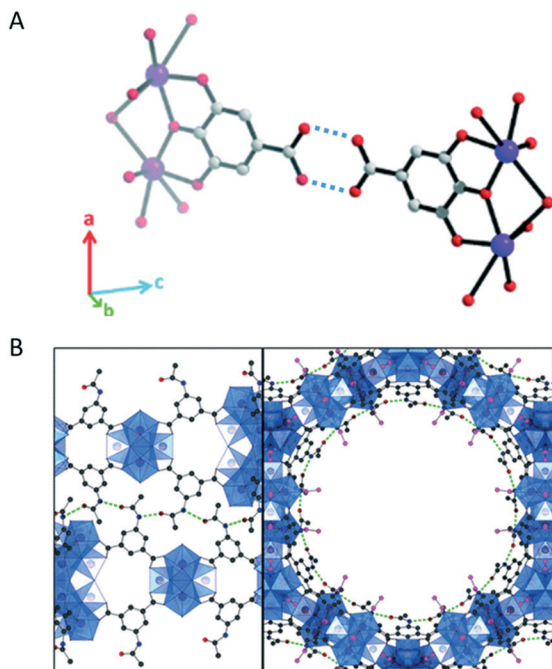
Fig. 7 (A) Hydrogen bonds (indicated by the dashed lines) between carboxylic acids in bismuth subgallate. Purple: Bi; red: O; grey: C. Hydrogen atoms have been omitted for clarity. Reproduced from ref. 17 with permission from the Royal Chemical Society, copyright 2017. (B) Stacked layers of CAU-45 connected by hydrogen bonds (dashed green lines) between the N–H and C=O groups. The layers are viewed along the [110] (left) and [001] (right) directions. Blue: Zr-oxo clusters; black: C from the linkers; pink; C from acetate; red: O; dark blue: N. Reproduced from ref. 108 with permission from the American Chemical Society, copyright 2019.

between the DABCO molecules and the framework, between the water molecules and the framework, and between the water molecules.

3.4. Crystal chirality

It is common that a target chiral compound resulted in a racemic mixture during the crystallization process. The tremendous interest in producing pure enantiomers make it necessary to develop characterization techniques for the determination of the absolute stereochemistry of nanocrystals. 3D ED takes the advantage of dynamical effects that arise from multiple scattering of electrons to break the inversion symmetry in reciprocal space. Brázda *et al.* has recently reported the determination of the absolute structure of a pharmaceutical cocrystal of sofosbuvir and L-proline by using PEDT (Fig. 8A).[111] The structure was solved *ab initio*, and by taking the inversion symmetry violation into account, the absolute structure was determined by comparing the final *R*-values of the enantiomers. In addition, studies using MicroED reported to determine the absolute configuration of natural products (Fig. 8B).[112,113] By attaching L-amino acids to the target molecules and collecting data with high tilting speed with minimized beam damage, the stereochemistry of
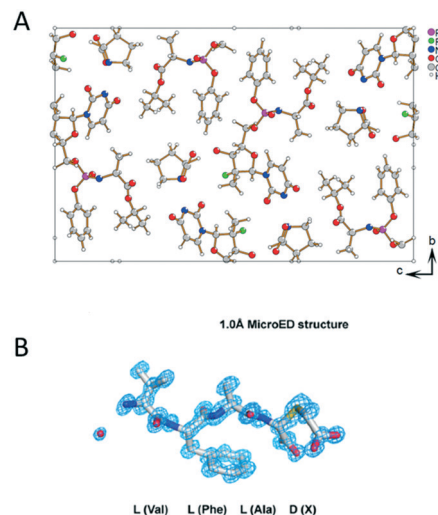

Fig. 8 (A) The structural model of sofosbuvir L-proline cocrystal determined by PEDT. Reproduced from ref. 111 with permission from the American Association for the Advancement of Science, copyright 2019. (B) MicroED structure of the D configuration of the 3-thiaGlu in the chemically synthesized tetrapeptides (VFAX, X = 3-thiaGlu). Reproduced from ref. 112 with permission from the American Association for the Advancement of Science, copyright 2019.

the unknown chiral center was deducted from the absolute configuration of the modified amino acids.

4. Summary and perspectives

In this highlight article, we describe the recent development of 3D ED methods, which offers the opportunity for characterizing nano- and submicro-sized crystals. We highlight the unique advantage of using 3D ED for single-crystal analysis from powder samples and give examples showing the obtained detailed structural information can yield a deep understanding on crystalline compounds, including revealing structure–property relationships, solving individual structures in phase mixtures, identifying hydrogen bonds, and determining absolute configuration of chiral crystals. This demonstrates that 3D ED as an important characterization tool for crystal engineering. Given the fast development and growing of this field, we foresee that 3D ED methods will become a widespread characterization technique used for understanding nano- and submicron-sized crystals, and the obtained knowledge will be crucial for exploring their new applications.

Nevertheless, as the development of 3D ED technique is still in the dawn, much improvement can be made to tackle the challenges it faces. It is currently difficult to prepare samples whose structures are only stable in organic liquids due to lack of such protocols. Additionally, the continuous 3D ED methods and their automation allow a fast and reliable data collection. Improvements towards fully automatic could further expand 3D ED accessibility to non-experts.

For structure determination, using kinematical approximation to treat 3D ED data can provide accurate and reliable results. However, dynamical effects cause reflection intensities deviate from their kinematical approximation, leading to relatively high R-values. Further developments, such as dynamical refinement,[66] are highly desired to tackle this challenge, especially for complicated crystal structures. Moreover, as a rather new method compared to X-ray crystallography, it is urgently needed to setup standards and guidelines for publishing and depositing 3D ED structures.

For studying crystals, although 3D ED can provide various structural details, localization of guest molecules in porous crystals is still a challenge. Currently, identify guest species by 3D ED requires to have high occupancy, high periodicity, and strong interactions to the host structure.[61,108] In addition, high vacuum in TEMs poses a challenge to damage the host–guest systems. Future development on 3D ED to locate and understand local behaviors of guest-species could open new opportunities for understanding and engineering porous crystals.

Conflicts of interest

There are no conflicts to declare.

Acknowledgements

Notes and references

1 W. H. Bragg and W. L. Bragg, *Proc. R. Soc. London, Ser. A*, 1913, **88**, 428–438.

2 C. R. Groom, I. J. Bruno, M. P. Lightfoot and S. C. Ward, *Acta Crystallogr., Sect. B: Struct. Sci., Cryst. Eng. Mater.*, 2016, **72**, 171–179.

3 A. Belsky, M. Hellenbrandt, V. L. Karen and P. Luksch, *Acta Crystallogr., Sect. B: Struct. Sci.*, 2002, **58**, 364–369.

4 S. Grazulis, D. Chateigner, R. T. Downs, A. F. T. Yokochi, M. Quirós, L. Lutterotti, E. Manakova, J. Butkus, P. Moeck and A. Le Bail, *J. Appl. Crystallogr.*, 2009, **42**, 726–729.

5 H. Furukawa, K. E. Cordova, M. O'Keeffe and O. M. Yaghi, *Science*, 2013, **341**, 1230444.

6 S. L. Childs and M. J. Zaworotko, *Cryst. Growth Des.*, 2009, **9**(6), 2950.

7 S. C. Capelli, H.-B. Bürgi, B. Dittrich, S. Grabowsky and D. Jayatilaka, *IUCrJ*, 2014, **1**, 367–379.

8 S. Parsons, H. D. Flack and T. Wagner, *Acta Crystallogr., Sect. B: Struct. Sci., Cryst. Eng. Mater.*, 2013, **69**, 249–259.

9 E. Mugnaioli, A. E. Lanza, G. Bortolozzi, L. Righi, M. Merlini, V. Cappello, L. Marini, A. Athanassiou and M. Gemmi, *ACS Cent. Sci.*, 2020, **6**, 1578–1586.

10 T. Gruene and E. Mugnaioli, *Chem. Rev.*, 2021, **121**, 11823–11834.

11 T. Gruene, J. J. Holstein, G. H. Clever and B. Keppler, *Nat. Rev. Chem.*, 2021, **5**, 660–668.

12 Z. Huang, E. S. Grape, J. Li, A. K. Inge and X. Zou, *Coord. Chem. Rev.*, 2021, **427**, 213583.

13 J. F. Bruhn, G. Scapin, A. Cheng, B. Q. Mercado, D. G. Waterman, T. Ganesh, S. Dallakyan, B. N. Read, T. Nieusma, K. W. Lucier, M. L. Mayer, N. J. Chiang, N. Poweleit, P. T. McGilvray, T. S. Wilson, M. Mashore, C. Hennessy, S. Thomson, B. Wang, C. S. Potter and B. Carragher, *Front. Mol. Biosci.*, 2021, **8**, 354.

14 U. Kolb, T. Gorelik, C. Kübel, M. T. Otten and D. Hubert, *Ultramicroscopy*, 2007, **107**, 507–513.

15 D. Zhang, P. Oleynikov, S. Hovmöller and X. Zou, *Z. Kristallogr.*, 2010, **225**, 94–102.

16 P. Boullay, L. Palatinus and N. Barrier, *Inorg. Chem.*, 2013, **52**, 6127–6135.

17 M. O. Cichocka, J. Ångström, B. Wang, X. Zou and S. Smeets, *J. Appl. Crystallogr.*, 2018, **51**(474), 1652–1661.

18 I. Nederlof, E. van Genderen, Y.-W. Li and J.-P. Abrahams, *Acta Crystallogr., Sect. D: Biol. Crystallogr.*, 2013, **69**, 1223–1230.

19 M. Gemmi and P. Oleynikov, *Z. Kristallogr.*, 2013, **228**, 51–58.

20 M. Gemmi, M. G. I. La Placa, A. S. Galanis, E. F. Rauch and S. Nicolopolus, *J. Appl. Crystallogr.*, 2015, **48**, 718–727.

21 S. Plana-Ruiza, Y. Krysiaka, J. Portillo, E. Alig, S. Estradé, F. Peiró and U. Kolb, *Ultramicroscopy*, 2020, **211**, 112951.

22 S. Kodjikian and H. Klein, *Ultramicroscopy*, 2019, **200**, 12–19.

23 B. L. Nannenga, D. Shi, A. G. W. Leslie and T. Gonen, *Nat. Methods*, 2014, **11**, 927–930.

24 J. A. Rodriguez, M. I. Ivanova, M. R. Sawaya, D. Cascio, F. E. Reyes, D. Shi, S. Sangwan, E. L. Guenther, L. M. Johnson, M. Zhang, L. Jiang, M. A. Arbing, B. L. Nannenga, J. Hattne, J. Whitelegge, A. S. Brewster, M. Messerschmidt, S. Boutet, N. K. Sauter, T. Gonen and D. S. Eisenberg, *Nature*, 2015, **525**, 486–490.

25 M. R. Sawaya, J. Rodriguez, D. Cascio, M. J. Collazo, D. Shi, F. E. Reyes, J. Hattne, T. Gonen and D. S. Eisenberg, *Proc. Natl. Acad. Sci. U. S. A.*, 2016, **113**, 11232–11236.

26 M. Gallagher-Jones, C. Glynn, D. R. Boyer, M. W. Martynowycz, E. Hernandez, J. Miao, C.-T. Zee, I. V. Novikova, L. Goldschmidt, H. T. McFarlane, G. F. Helguera, J. E. Evans, M. R. Sawaya, D. Cascio, D. S. Eisenberg, T. Gonen and J. A. Rodriguez, *Mol. Biol.*, 2018, **25**, 131–134.

27 E. L. Guenther, P. Ge, H. Trinh, M. R. Sawaya, D. Cascio, D. R. Boyer, T. Gonen, Z. H. Zhou and D. S. Eisenberg, *Nat. Struct. Mol. Biol.*, 2018, **25**, 311–319.

28 C.-T. Zee, C. Glynn, M. Gallagher-Jones, J. Miao, C. G. Santiago, D. Cascio, T. Gonen, M. R. Sawaya and J. A. Rodriguez, *IUCrJ*, 2019, **6**, 197–205.

29 W. Kabsch, *Acta Crystallogr., Sect. D: Biol. Crystallogr.*, 2010, **66**, 125–132.

30 T. G. G. Battye, L. Kontogiannis, O. Johnson, H. R. Powell and A. G. W. Leslie, *Acta Crystallogr., Sect. D: Biol. Crystallogr.*, 2011, **67**, 271–281.

31 M. T. B. Clabbers, T. Gruene, J. M. Parkhurst, J. P. Abrahams and D. G. Waterman, *Acta Crystallogr., Sect. D: Struct. Biol.*, 2018, **74**, 506–518.

32 L. Palatinus, P. Brázda, M. Jelínek, J. Hrdá, G. Steciuk and M. Klementová, *Acta Crystallogr., Sect. B: Struct. Sci., Cryst. Eng. Mater.*, 2019, **75**, 512–522.

33 G. M. Sheldrick, *Acta Crystallogr., Sect. A: Found. Crystallogr.*, 2008, **71**, 112–122.

34 M. C. Burla, *J. Appl. Crystallogr.*, 2015, **48**, 306–309.

35 L. Palatinus and G. Chapuis, *J. Appl. Crystallogr.*, 2007, **40**, 786–790.

36 G. M. Sheldrick, *Acta Crystallogr., Sect. A: Found. Adv.*, 2015, **71**, 3–8.

37 C. B. Hübschle, G. M. Sheldrick and B. Dittrich, *J. Appl. Crystallogr.*, 2011, **44**, 1281–1284.

38 A. Thorn, B. Dittrich and G. M. Sheldrick, *Acta Crystallogr., Sect. A: Found. Crystallogr.*, 2012, **68**, 448–451.

39 V. Petříček, M. Dušek and L. Palatinus, *Z. Kristallogr.*, 2014, **229**, 345–352.

40 V. Petricek, V. Eigner, M. Dusek and A. Cejchan, *Z. Kristallogr.*, 2016, **231**, 301–312.

41 V. Petricek, M. Dusek and J. Plasil, *Z. Kristallogr.*, 2016, **231**, 583–599.

42 I. Goldberg, *CrystEngComm*, 2008, **10**, 637–645; J. Huan, X. Zhang and Q. Zeng, *Phys. Chem. Chem. Phys.*, 2019, **21**, 11537–11553.

43 E. Mugnaioli, T. Gorelik and U. Kolb, *Ultramicroscopy*, 2009, **109**, 758–765.

44 U. Kolb, E. Mugnaioli and T. E. Gorelik, *Cryst. Res. Technol.*, 2011, **46**, 542–554.

45 W. Wan, J. Sun, J. Su, S. Hovmöller and X. Zou, *J. Appl. Crystallogr.*, 2013, **46**, 1863–1873.

46 R. Vincent and P. A. Midgley, *Ultramicroscopy*, 1994, **53**, 271–282.

47 D. Denysenko, M. Grzywa, M. Tonigold, B. Streppel, I. Krkljus, M. Hirscher, E. Mugnaioli, U. Kolb, J. Hanss and D. Volkmer, *Chem. – Eur. J.*, 2011, **17**, 1837–1848.

48 M. Feyand, E. Mugnaioli, F. Vermoortele, B. Bueken, J. M. Dieterich, T. Reimer, U. Kolb, D. de Vos and N. Stock, *Angew. Chem., Int. Ed.*, 2012, **51**, 10373–10376.

49 D. Feng, T.-F. Liu, J. Su, M. Bosch, Z. Wei, W. Wan, D. Yuan, Y.-P. Chen, X. Wang, K. Wang, X. Lian, Z.-Y. Gu, J. Park, X. Zou and H.-C. Zhou, *Nat. Commun.*, 2015, **6**, 1–8.

50 D. Feng, K. Wang, J. Su, T.-F. Liu, J. Park, Z. Wei, M. Bosch, A. Yakovenko, X. Zou and H.-C. Zhou, *Angew. Chem., Int. Ed.*, 2015, **54**, 149–154.

51 Q. Zhang, J. Su, D. Feng, Z. Wei, X. Zou and H.-C. Zhou, *J. Am. Chem. Soc.*, 2015, **137**, 10064–10067.

52 Q. Yao, A. Bermejo Gómez, J. Su, V. Pascanu, Y. Yun, H. Zheng, H. Chen, L. Liu, H. N. Abdelhamid, B. Martín-Matute and X. Zou, *Chem. Mater.*, 2015, **27**, 5332–5339.

53 N. Portolés-Gil, A. Lanza, N. Aliaga-Alcalde, J. A. Ayllón, M. Gemmi, E. Mugnaioli, A. M. López-Periago and C. Domingo, *ACS Sustainable Chem. Eng.*, 2018, **6**, 12309–12319.

54 Y.-B. Zhang, J. Su, H. Furukawa, Y. Yun, F. Gándara, A. Duong, X. Zou and O. M. Yaghi, *J. Am. Chem. Soc.*, 2013, **135**, 16336–16339.

55 E. van Genderen, M. T. B. Clabbers, P. P. Das, A. Stewart, I. Nederlof, K. C. Barentsen, Q. Portillo, N. S. Pannu, S. Nicolopoulos, T. Gruene and J. P. Abrahams, *Acta Crystallogr., Sect. A: Found. Adv.*, 2016, **72**, 236–242.

56 G. Tinti, E. Fröjdh, E. van Genderen, T. Gruene, B. Schmitt, D. A. M. de Winter, B. M. Weckhuysen and J. P. Abrahams, *IUCrJ*, 2018, **5**, 190–199.

57 K. Naydenova, G. McMullan, M. J. Peet, Y. Lee, P. C. Edwards, S. Chen, E. Leahy, S. Scotcher, R. Henderson and C. Russo, *IUCrJ*, 2019, **6**, 1086–1098.

58 S. Smeets, B. Wang, M. O. Cichocka, J. Ångström and W. Wan, Instamatic, Zenodo, 2019, DOI: 10.5281/zenodo.3470096.

59 M. Ge, T. Yang, Y. Wang, F. Carraro, W. Liang, C. Doonan, P. Falcaro, H. Zheng, X. Zou and Z. Huang, *Faraday Discuss.*, 2021, **231**, 66–80.

60 S. Smeets and W. Wang, *J. Appl. Crystallogr.*, 2017, **50**, 885–892.

61 B. Wang, T. Rhauderwiek, A. K. Inge, H. Xu, T. Yang, Z. Huang, N. Stock and X. Zou, *Chem. – Eur. J.*, 2018, **24**, 17429–17433.

62 Y. Wang, T. Yang, H. Xu, X. Zou and W. Wan, *J. Appl. Crystallogr.*, 2018, **51**, 1094–1101.

63 L. Samperisi, A. Jaworski, G. Kaur, K. P. Lillerud, X. Zou and Z. Huang, *J. Am. Chem. Soc.*, 2021, **143**(43), 17947–17952.

64 Z. Huang, M. Ge, F. Carraro, C. J. Doonan, P. Falcaro and X. Zou, *Faraday Discuss.*, 2021, **225**, 118–132.

65 S. A. Basnayake, J. Su, X. Zou and K. J. Balkus, *Inorg. Chem.*, 2015, **54**, 1816–1821.

66 L. Palatinus, V. Petříček and C. Antunes Corrêa, *Acta Crystallogr., Sect. A: Found. Adv.*, 2015, **71**, 235–244.

67 L. Palatinus, C. A. Corrêa, G. Steciuk, D. Jacob, P. Roussel, P. Boullay, M. Klemantová, M. Gemmi, J. Kopeček, M. C. Domeneghetti, F. Cámara and V. Petříček, *Acta Crystallogr., Sect. B: Struct. Sci., Cryst. Eng. Mater.*, 2015, **71**, 740–751.

68 Y.-B. Zhang, J. Su, H. Furukawa, Y. Yun, F. Gándare, A. Duong, X. Zou and O. M. Yaghi, *J. Am. Chem. Soc.*, 2013, **135**, 16336–16339.

69 P. Cui, E. S. Grape, P. R. Spackman, Y. Wu, R. Clowes, G. M. Day, A. K. Inge, M. A. Little and A. Cooper, *J. Am. Chem. Soc.*, 2020, **142**, 12743–12750.

70 Z. Huang, T. Willhammar and X. Zou, *Chem. Sci.*, 2021, **12**, 1206.

71 J. Dubochet, M. Adrian, J. J. Chang, J. C. Homo, J. Lepault and A. W. McDowall, *Q. Rev. Biophys.*, 1988, **21**, 129–228.

72 K. A. Taylor and R. M. Glasser, *J. Ultrastruct. Res.*, 1976, **55**, 448–456.

73 J. Zhao, H. Xu, H. Lebrette, M. Carroni, H. Taberman, M. Högbom and X. Zou, *Nat. Commun.*, 2021, **12**, 5036.

74 A. Schneemann, V. Bon, I. Schwedler, I. Senkovska, S. Kaskel and R. A. Fischer, *Chem. Soc. Rev.*, 2014, **43**(16),

6062–6096; R. E. Morris and L. Brammer, *Chem. Soc. Rev.*, 2017, **46**(17), 5444–5462.

75 J.-R. Li, J. Sculley and H.-C. Zhou, *Chem. Rev.*, 2012, **112**, 869–932.

76 L. E. Kreno, K. Leong, O. K. Farha, M. Allendorf, R. P. Van Duyne and J. T. Hupp, *Chem. Rev.*, 2012, **112**, 1105–1125.

77 Z. Hu, B. J. Deibert and J. Li, *Chem. Soc. Rev.*, 2014, **43**, 5815–5840; K. Lu, T. Aung, N. Guo, R. Weichselbaum and W. Lin, *Adv. Mater.*, 2018, **30**, 1707634.

78 T. Zhang and W. Lin, *Chem. Soc. Rev.*, 2014, **43**, 5982–5993.

79 J. Della Rocca, D. Liu and W. Lin, *Acc. Chem. Res.*, 2011, **44**, 957–968; W. Xuan, C. Zhu, Y. Liu and Y. Cui, *Chem. Soc. Rev.*, 2012, **41**, 1677–1695.

80 J. Hynek, P. Dr, Dr Brázda, J. Rohlíček, M. G. S. Dr, Dr Londesborough and J. Demel, *Angew. Chem., Int. Ed.*, 2018, **57**, 5016.

81 S. Smolders, T. Willhammar, A. Krajnc, K. Sentosun, M. T. Wharmby, K. A. Lomachenko, S. Bals, G. Mali, M. B. J. Roeffaers, D. E. De Vos and B. Bueken, *Angew. Chem.*, 2019, **131**, 9258–9263.

82 F. M. Amombo Noa, E. Svensson Grape, S. M. Brülls, O. Cheung, P. Malmberg, A. K. Inge, C. J. McKenzie, J. Mårtensson and L. Öhrström, *J. Am. Chem. Soc.*, 2020, **142**, 9471–9481.

83 M. O. Cichocka, Z. Liang, D. Feng, S. Back, S. Siahrostami, X. Wang, L. Samperisi, Y. Sun, H. Xu, N. Hedin, H. Zheng, X. Zou, H.-C. Zhou and Z. Huang, *J. Am. Chem. Soc.*, 2020, **142**, 15386–15395.

84 F. Banihashemia, G. Buab, A. Thakera, D. Williams, J. Y. S. Lina and B. L. Nannenga, *Ultramicroscopy*, 2020, **216**, 113048.

85 J.-H. Dou, M. Q. Arguilla, Y. Luo, J. Li, W. Zhang, L. Sun, J. L. Mancuso, L. Yang, T. Chen, L. R. Parent, G. Skorupskii, N. J. Libretto, C. Sun, M. C. Yang, P. V. Dip, E. J. Brignole, J. T. Miller, J. Kong, C. H. Hendon, J. Sun and M. Dincă, *Nat. Mater.*, 2021, **20**, 222–228.

86 D. Feng, T.-F. Liu, J. Su, M. Bosch, Z. Wei, W. Wan, D. Yuan, Y.-P. Chen, X. Wang, K. Wang, X. Lian, Z.-Y. Gu, J. Park, X. Zou and H.-C. Zhou, *Nat. Commun.*, 2015, **6**, 1–8.

87 D. Feng, K. Wang, J. Su, T.-F. Liu, J. Park, Z. Wei, M. Bosch, A. Yakovenko, X. Zou and H.-C. Zhou, *Angew. Chem., Int. Ed.*, 2015, **54**, 149–154.

88 Q. Zhang, J. Su, D. Feng, Z. Wei, X. Zou and H.-C. Zhou, *J. Am. Chem. Soc.*, 2015, **137**, 10064–10067.

89 D. Lenzen, J. Zhao, S. J. Ernst, M. Wahiduzzaman, A. Ken Inge, D. Fröhlich, H. Xu, H. J. Bart, C. Janiak, S. Henninger, G. Maurin, X. Zou and N. Stock, *Nat. Commun.*, 2019, **10**, 3025.

90 S. Yuan, J.-S. Qin, H.-Q. Xu, J. Su, D. Rossi, Y. Chen, L. Zhang, C. Lollar, Q. Wang, H.-L. Jiang, D. H. Son, H. Xu, Z. Huang, X. Zou and H.-C. Zhou, *ACS Cent. Sci.*, 2018, **4**, 105–111.

91 T. Gorelik, M. U. Schmidt, J. Brüning, S. Beko and U. Kolb, *Cryst. Growth Des.*, 2009, **9**, 3898–3903.

92 Y. Yun, W. Wan, F. Rabbani, J. Su, H. Xu, S. Hovmöller, M. Johnsson and X. Zou, *J. Appl. Crystallogr.*, 2014, **47**, 2048–2054.

93 G. C. Capitani, E. Mugnaioli, J. Rius, P. Gentile, T. Catelani, A. Lucotti and U. Kolb, *Am. Mineral.*, 2014, **99**, 500–510.

94 M. Ge, Y. Wang, F. Carraro, W. Liang, M. Roostaeinia, S. Siahrostami, D. M. Proserpio, C. Doonan, P. Falcaro, H. Zheng, X. Zou and Z. Huang, *Angew. Chem., Int. Ed.*, 2021, **60**, 11391–11397.

95 B. Wang, X. Zou and S. Smeets, *IUCrJ*, 2019, **6**, 854–867.

96 E. T. Broadhurst, H. Xu, M. T. B. Clabbers, M. Lightowler, F. Nudelman, X. Zoub and S. Parsons, *IUCrJ*, 2020, **7**, 5–9.

97 E. T. Broadhurst, H. Xu, S. Parsons and F. Nudelman, *IUCrJ*, 2021, **8**, 860–866.

98 C. G. Jones, M. W. Martynowycz, J. Hattne, T. J. Fulton, B. M. Stoltz, J. A. Rodriguez, H. M. Nelson and T. Gonen, *ACS Cent. Sci.*, 2018, **4**, 1587–1592.

99 U. Kolb, T. E. Gorelik, E. Mugnaioli and A. Stewart, *Polym. Rev.*, 2010, **50**, 385–409.

100 T. Gruene, J. T. C. Wennmacher, C. Zaubitzer, J. J. Holstein, J. Heidler, A. Fecteau-Lefebvre, S. De Carlo, E. Müller, K. N. Goldie, I. Regeni, T. Li, G. Santiso-Quinones, G. Steinfeld, S. Handschin, E. van Genderen, J. A. van Bokhoven, G. H. Clever and R. Pantelic, *Angew. Chem., Int. Ed.*, 2018, **57**, 16313–16317.

101 P. P. Das, I. Andrusenko, E. Mugnaioli, J. A. Kaduk, S. Nicolopoulos, M. Gemmi, N. C. Boaz, A. M. Gindhart and T. Blanton, *Cryst. Growth Des.*, 2021, **21**, 2019–2027.

102 I. Andrusenko, V. Hamilton, E. Mugnaioli, A. Lanza, C. Hall, J. Potticary, S. R. Hall and M. Gemmi, *Angew. Chem., Int. Ed.*, 2019, **58**, 10919–10922.

103 F. Papi, J. Potticary, A. E. Lanza, S. R. Hall and M. Gemmi, *Cryst. Growth Des.*, 2021, **21**(11), 6341–6348.

104 C. L. Hall, I. Andrusenko, J. Potticary, S. Gao, X. Liu, W. Schmidt, N. Marom, E. Mugnaioli, M. Gemmi and S. R. Hall, *ChemPhysChem*, 2021, **22**, 1631–1637.

105 B. Moulton and M. J. Zaworotko, *Chem. Rev.*, 2001, **101**, 1629–1658.

106 L. Palatinus, P. Brázda, P. Boullay, O. Perez, M. Klementová, S. Petit, V. Eigner, M. Zaarour and S. Mintova, *Science*, 2017, **355**, 166–169.

107 M. T. B. Clabbers, T. Gruene, E. vanGenderen and J. P. Abrahams, *Acta Crystallogr., Sect. A: Found. Adv.*, 2019, **75**, 82–93.

108 S. Leubner, V. E. G. Bengtsson, K. Synnatschke, J. Gosch, A. Koch, H. Reinsch, H. Xu, C. Backes, X. Zou and N. J. Stock, *J. Am. Chem. Soc.*, 2020, **142**, 15995–16000.

109 H.-S. Xu, Y. Luo, X. Li, P. Z. See, Z. Chen, T. Ma, L. Liang, K. Leng, I. Abdelwahab, L. Wang, R. Li, X. Shi, Y. Zhou, X. F. Lu, X. Zhao, C. Liu, J. Sun and K. P. Loh, *Nat. Commun.*, 2020, **11**, 1–6.

110 J. Zhu, L. Samperisi, M. Kalaj, J. A. Chiong, J. B. Bailey, Z. Zhang, C.-J. Yu, R. E. Sikma, X. Zou, S. M.

Cohen, Z. Huang and F. A. Tezcan, *Dalton Trans.*, 2022, **51**, 1927–1935.

111 P. Brázda, L. Palatinus and M. Babor, *Science*, 2019, **364**, 667–669.

112 C. P. Ting, M. A. Funk, S. L. Halaby, Z. Zhang, T. Gonen and W. A. van der Donk, *Science*, 2019, **365**, 280–284.

113 M. Dick, N. S. Sarai, M. W. Martynowycz, T. Gonen and F. H. Arnold, *J. Am. Chem. Soc.*, 2019, **141**, 19817–19822.